A Novel Architecture of Multimode Hybrid Powertrains for Fuel Efficiency and Sizing Optimization

HYUKJOON KWON, YEONGIL CHOI, WOULSUN CHOI, AND SEUNGWOOK LEE
Hyundai Motor Company Research and Development Center, Hwaseong-si 18280, South Korea
Corresponding author: Hyukjoon Kwon (hkwon@hyundai.com)

ABSTRACT Hybrid powertrains have widely been developed as eco-friendly system and commercialized in the passenger vehicle market with clear benefits over conventional powertrains. Accordingly, there have been various research topics on architectures of hybrid power systems to further improve the system performance ability and sizing optimization for the packaging and production cost reduction. In this study, a novel multimode power split hybrid architecture has been suggested, which is based on multiple driving modes such as input- and output-power split and parallel hybrid modes in order to achieve fuel efficiency improvement and sizing optimization. The performance ability and sizing aspects of the invented system have been analyzed in comparison with Toyota Hybrid System (THS), which is a kind of typical power split hybrid architecture. The fuel efficiency of the suggested system has been compared by a backward-facing simulation with Dynamic Programming (DP) for representative driving test cycles from Environmental Protection Agency (EPA). In terms of the component sizing, the maximum torque and speed variation trends of motors have been analyzed according to the velocity variation. In the simulation and analysis results, the invented system shows opportunities to improve fuel efficiency with multiple driving modes and to reduce component sizing of power electronics which is related to the production cost reduction as well as the vehicle packaging space minimization.

INDEX TERMS Hybrid power systems, dynamic programming, fuel efficiency, power split hybrid transmission.

NOMENCLATURE

BSFC	Brake-Specific Fuel Consumption.
DHT	Dedicated Hybrid Transmission.
DP	Dynamic Programming.
DSHS	Dual Split Hybrid System.
EPA	Environmental Protection Agency.
FTP	Federal Test Procedure.
HEV	Hybrid Electric Vehicle.
HWFET	Highway Fuel Economy Test.
MG	Motor and Generator Unit.
SOC	State of Charge.
THS	Toyota Hybrid System.
UDDS	Urban Dynamometer Driving Schedule.

The associate editor coordinating the review of this manuscript and approving it for publication was Qiuye Sun.

I. INTRODUCTION

Eco-friendly vehicles such as hybrid vehicles and pure electric vehicles have widely been researched and developed by most automotive companies due to the reasons like the unstable oil price and the environmental regulations by governments. According to the current situation, hybrid electric vehicles (HEVs), among the different kinds of eco-friendly vehicles, are currently the most popular alternatives to conventional vehicles. Multiple types of hybrid systems have been commercialized by automotive manufacturers in the passenger vehicle market.

There have been various research topics related to hybrid vehicle systems. The research topics of the recent studies include diverse research areas such as driving and regenerative control strategy of HEVs [1]–[3], optimal design of component sizing and electrical energy storage [4], [5], driving energy management strategy for HEV [6], a design methodology for compound-split hybrid electric vehicles

with the compound lever diagram [7], comparative analysis of classical energy management optimization with reinforcement learning [8], a parametric model for power split hybrid transmissions [9], and thermal management and analysis of electrified drive systems and hydraulic hybrids [10]–[13]. For the research on architectures of hybrid systems, there have existed a number of studies for past decades since the 1970s and diverse recent studies like a multimode power split hybrid transmission [14], hybrid powertrain architectures for a four-wheel drive [15], series-parallel and power split architecture based dedicated hybrid transmissions (DHTs) [16], powertrain configuration of single motor hybrid systems [17], and novel powertrain architectures with Ravigneaux and planetary gear trains [18].

In this study, a hybrid architecture based on multiple driving modes with power split and parallel hybrid modes, named Dual Split Hybrid System (DSHS), has been studied in order to analyze the performance ability and other aspects. The invented system has been compared with Toyota Hybrid System (THS), which is a typical power split hybrid system, in terms of the performance ability and component sizing aspects. In order to analyze the performance ability, both systems have been simulated by a backward-facing method with Dynamic Programming (DP) for Urban Dynamometer Driving Schedule (UDDS), which is also called FTP-72, and Highway Fuel Economy Test (HWFET), which are among the representative Environmental Protection Agency (EPA) driving test cycles. The component sizing aspect has been compared by analysis of the torque and speed variation of motors according to an example driving case. The potential and advantages of DSHS have been described in comparison with THS and discussed with the results from the simulation and analysis.

II. SYSTEM DESCRIPTION

Architectures for hybrid vehicles can mainly be divided into series, parallel, and power-split systems according to how the power paths are constructed. The suggested novel architecture consists of multiple different driving modes such as power split and parallel hybrid modes.

The power split hybrid system is mainly classified into two architectures; the input-split (or output-coupled) power split and output-split (or input-coupled) power split systems. For both systems, three mechanical paths from a planetary gear train are connected to the engine, the final drive, and a motor, respectively. The difference is the location of the secondary motor. A motor is mechanically coupled with the path of the final drive for the input-split system, while for the output-split system, a motor is connected to the mechanical path between the engine and the planetary gear train.

The mechanical layout difference between input- and output-split power split architectures results in different power distribution and system efficiency according to the speed ratio between the engine and the final drive [19]–[21]. The driving modes of power split hybrid systems can mainly

be divided into power additive, full mechanical, and power recirculation modes.

When the system is under the power additive mode with the power ratio between the electrical and mechanical paths greater than zero, the power flow from the engine splits into the mechanical and electrical paths.

For the power recirculation mode with a power ratio between the electrical and mechanical paths less than zero, a part of the power from the mechanical path recirculates through the electrical path and is delivered again through the mechanical path. The power recirculation is undesirable because the system efficiency gets worse as the amount of power recirculation through the electrical path increases.
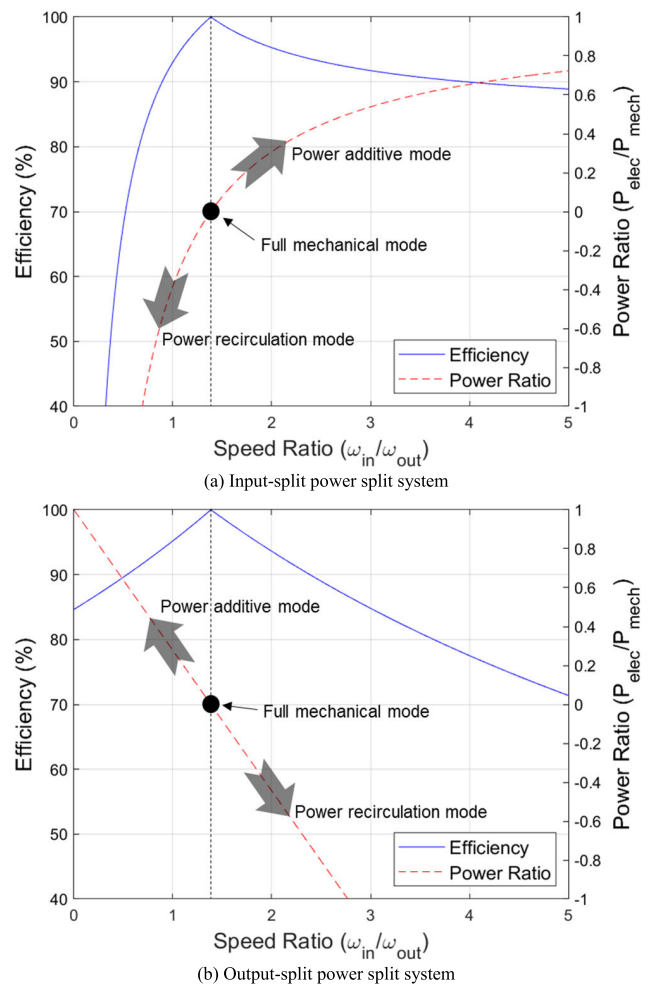

FIGURE 1. Hybrid system efficiency and power path ratio for input- and output-split power split transmissions.

When there is no power through the electrical path, the system is under the full mechanical mode, which shows the highest efficiency among the three modes due to no electrical power loss. The input- and output-split power split hybrids have different driving modes according to the speed ratio and it results in a different system efficiency distribution.

Fig. 1 shows the hybrid system efficiency and power path ratio for the power split hybrid transmissions according to

the speed ratio, which is drawn with assumptions of the constant motor efficiency and standing gear ratio of 2.6 for the planetary gear train. Fig. 1 (a) and (b) are figures for the input-split power split system and the output-split power split system, respectively. The trends of efficiency and power ratio for input- and output-split power split systems are different according to the speed ratio of the engine and wheel speeds. As expected, both systems have the highest efficiency when the speed ratio is the full mechanical point of 1.385 with the full mechanical mode. When the speed ratio is greater than the full mechanical point, the input-split power split system is under the power additive mode, while the output-split power split system is under power recirculation mode. On the other hand, when the power speed ratio is less than the full mechanical point, the input- and output-split power split systems have the power recirculation and power additive modes, respectively.

Since the efficiency of the power additive mode is higher than that of the power recirculation mode in general, the input-split power split system has higher system efficiency compared to the output-power split hybrid system for the speed ratio greater than the full mechanical point. On the other hand, the output-split power split hybrid system shows higher efficiency than the input-split power split system for the speed ratio less than the full mechanical point.

Typical examples of the input- and output split power split systems are THS and Chevrolet Volt, respectively [22], [23]. As described, since the output-split power split system has relatively low efficiency for the low vehicle speed, the output-split power split system usually includes another driving mode for the low vehicle speed such as full electric and series hybrid modes.
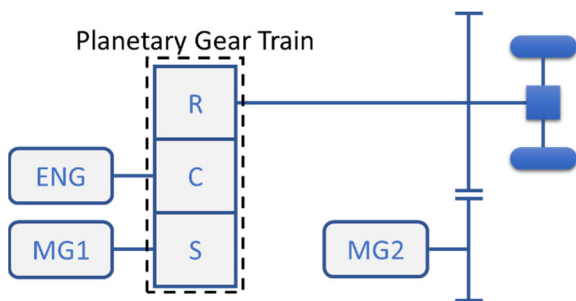

FIGURE 2. Power split hybrid architecture with an input-split hybrid mode (Toyota hybrid system).

There are 12 possible power split architectures for the power split hybrid systems with a planetary gear train [24]. THS is based on an input-split power split transmission among them. Fig. 2 shows the schematic of the power split hybrid architecture for THS with a single planetary gear train, where R is the ring gear, C is the carrier, and S is the sun gear. The engine, final drive, and MG-1 are connected to the carrier, ring gear, and sun gear of the planetary gear train, respectively. MG-2 is coupled with the mechanical path by an external gear between the ring gear and the final drive.

The invented hybrid architecture, DSHS, consists of multiple driving modes including input- and output-split power split hybrid modes. The architecture of DSHS is similar to THS in terms of the mechanical connections of the planetary gear train to the engine, final drive, and MG-1.
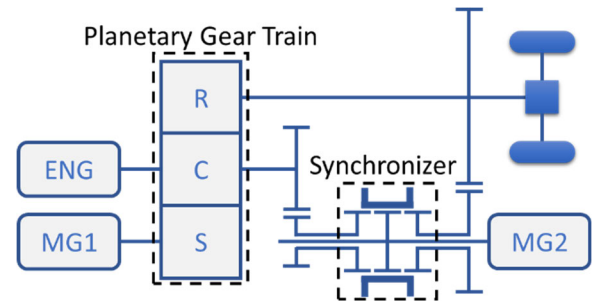

FIGURE 3. Multimode power split hybrid architecture with input- and output-split hybrid modes (dual split hybrid system).

Fig. 3 shows the schematic of the power split hybrid architecture for DSHS. The structural difference from THS is that a mechanical synchronizer is connected between the carrier of the planetary gear train and MG-2. DSHS has the
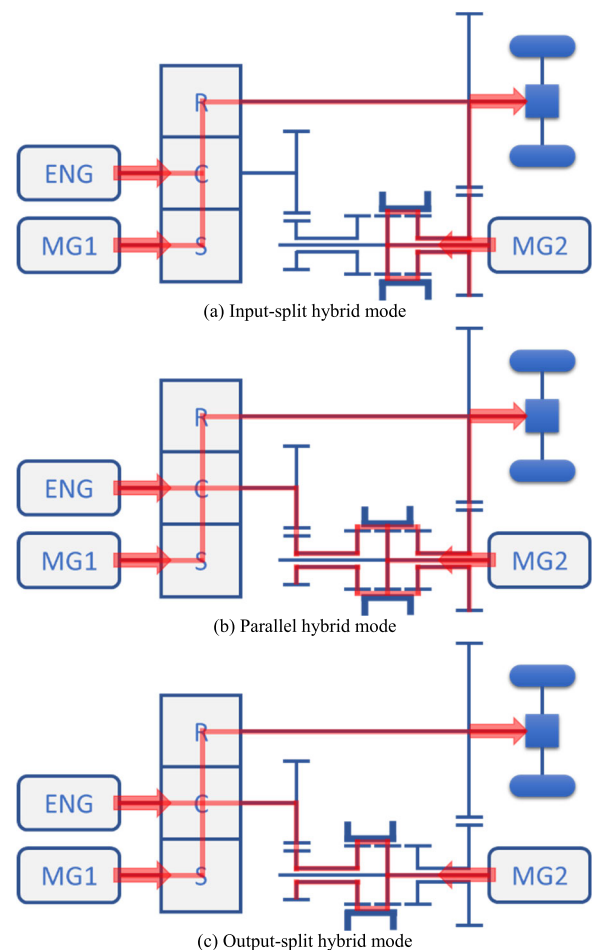

(a) Input-split hybrid mode

(b) Parallel hybrid mode

(c) Output-split hybrid mode

FIGURE 4. Power flow diagram for different driving modes of dual split hybrid system.

parallel and output-split power split hybrid modes in addition to the input-split power split hybrid mode by just adding a mechanical synchronizer to the typical architecture of THS.

Fig. 4 shows the power flow diagram for different driving modes of DSHS, which includes three different driving modes. First, when the mechanical path of the mechanical synchronizer is connected to the right side, MG-2 is coupled with the final drive and the system operates as an input-split power split hybrid transmission as shown in Fig. 4 (a). Second, if the sleeve of the mechanical synchronizer is in the neutral position, MG-2 is connected to both the final drive and the carrier of the planetary gear train as in Fig. 4 (b). As a result, the speed ratio between the engine and final drive becomes constant and the system operates as a parallel hybrid transmission. Lastly, as in Fig. 4 (c), when the sleeve of the mechanical synchronizer is connected to the left side, MG-2 is connected to the carrier of the planetary gear train, which makes the system work as an output-split power split hybrid transmission.

Since the driving modes of DSHS involve multiple hybrid modes, the fuel economy can be improved by using different driving modes for the different driving conditions. Even though there have been several studies on multimode hybrid systems, DSHS has a relatively simple structure compared to other multimode hybrid transmissions. DSHS uses only a mechanical synchronizer in addition to the structure of THS in order to achieve multiple kinds of hybrid driving modes. Another advantage of DSHS is that the sizing of the electrical components can be reduced because the amount of the power through the electrical path is less than other typical power split hybrid transmissions like THS. The detailed analysis results and discussion for the fuel efficiency and component sizing are described in the following sections.

III. ANALYSIS METHOD

The backward-facing simulation was applied with DP for the fuel economy analysis of the systems, which can provide globally optimized solutions for the given driving test cycles. Since the purpose of the study is the performance analysis of the suggested system, the methods in recent studies were not been applied in this paper [8], [25]. In the backward-facing simulation, the speed and torque of components are calculated from the vehicle speed data without driver models [26]. The wheel speed is obtained from the driving test cycle and the wheel demand torque is calculated by the derivative of the vehicle speed, which are used for the vehicle dynamics during the system modeling.

A. SYSTEM MODELING
For the vehicle dynamics, the required wheel traction force can be calculated from the force balance equation, which is given by,

$$ma = F_t + F_g + F_r + F_D \qquad (1)$$

where m is the mass of the vehicle, a is the acceleration of the vehicle, F_t is the traction force, F_g is the gravitational force,

F_r is the rolling resistance, and F_D is the aerodynamic drag. The traction force, gravitation force, rolling resistance, and aerodynamic drag can be expressed as,

$$F_t = \frac{M_w}{r_{dyn}} \qquad (2)$$

$$F_g = -mg\sin\theta \qquad (3)$$

$$F_r = -C_r \cdot mg\cos\theta \qquad (4)$$

$$F_D = -\frac{1}{2}\rho A_f C_d v^2 \qquad (5)$$

where M_w is torque loaded on the wheel, r_{dyn} is the wheel dynamic radius, g is the gravitational acceleration, θ is the angle of the slope, C_r is the rolling resistance coefficient, ρ is the density of the air, A_f is the frontal area of the vehicle, C_d is the drag coefficient of the vehicle, and v is the velocity of the vehicle.

Table 1 shows the simulation conditions for vehicle dynamics. The weight and road load coefficient are chosen from EPA fuel economy test data for Toyota Prius Prime with the model year of 2020 [27].

TABLE 1. Simulation conditions for vehicle dynamics.

Weight	1,644 kg
Road Load Coefficient	
f0	83.7 N
f1	3.75 N / (m/s)
f2	0.26 N / (m/s)²
Wheel Dynamic Radius	0.3 m

The planetary gear train can be modeled by the speed and torque relation equations as,

$$(1 + h)\,\omega_C = \omega_S + h\omega_R \qquad (6)$$

$$\tau_S : \tau_C : \tau_R = 1 : -(1 + h) : h \qquad (7)$$

where h is the standing gear ratio of the planetary gear train, ω_C is the angular speed of the gear carrier, ω_S is the angular speed of the sun gear, ω_R is the angular speed of the ring gear, τ_S is the torque on the sun gear, τ_C is the torque on the gear carrier, and τ_R is the torque on the ring gear. For the speed, at least two speed values need to be determined, and then, the rest speed can be obtained from (6). On the other hand, for the torque, once any torque of the sun gear, the carrier, and the ring gear is determined, the other two values can be calculated from (7).

The fuel consumption of the engine was calculated by the brake-specific fuel consumption (BSFC) map with engine speed and torque, which is based on the empirical data. The efficiency of the motors was also determined empirically with the efficiency map by the motor speed and torque. The temporary manipulated map data were used for the engine and motor, which are not the same as the map data for the production car.

A battery model with empirical data is used for obtaining the state-of-charge (SOC) variation. Once the battery demand

power is calculated from the engine and motor models with vehicle dynamics, the derivative of SOC can be calculated as follows [28],

$$S\dot{O}C = \frac{V_{OC} - \sqrt{V_{OC}^2 - 4R_{in}P_{bat}}}{2R_{in}I_{bat}} \qquad (8)$$

where $S\dot{O}C$ is the balance rate of the state-of-charge, V_{OC} is the open circuit voltage of the battery, R_{in} is the internal resistance of the battery, P_{bat} is the battery power exchange with electric components, and I_{bat} is the current from the battery. The open circuit voltage and internal resistance can be obtained with empirical relation data, which are expressed as a function of SOC.

B. OPTIMAL CONTROL MANAGEMENT

In this study, DP was used for describing the optimal control policy of the simulation models, which guarantees global optimal solutions, even though it requires heavier computational time compared to other optimization methods. According to Bellman's principle of optimality, the remaining decisions must include optimal policies for the states resulting from the beforehand decisions [29]. The time step of the given driving test cycle is divided into N stages and the transition function can be expressed as follows [30],

$$x(k+1) = f(x(k), u(k)) \qquad (9)$$

where x is the state variables, u is the control variable, and k is the stage of time.

The optimization problem for DP can be formulated by the choice of control variables at each state to find the optimal value of the objective function. The objective function can be expressed as [28], [31], [32],

$$J^* = min \sum_{t_0}^{t_{end}} L(x(k), u(k)) \qquad (10)$$

where J is the objective function, and L is the instantaneous cost function. The instantaneous cost function includes the instantaneous fuel consumption rate and penalty function which is given by,

$$L = \dot{m}_{fuel} + f_p \qquad (11)$$

where $\dot{m}_{fuel}$ is the instantaneous fuel consumption rate and f_p is the instantaneous penalty function. In this study, fuel consumption during the engine start-up was considered in the penalty function in order to prevent the engine from starting frequently.

IV. RESULTS AND DISCUSSION

The performance ability and component design aspects of DSHS have been analyzed in comparison with THS. For the performance analysis, both systems have been simulated by the backward-facing modeling with the energy management strategy by using DP approach. The electrical component sizing aspects have been analyzed in terms of the required power and torque of the electric motors with an example case study.

A. PERFORMANCE ANALYSIS

The engine operating points were observed with the engine BSFC map in order to check the simulation control optimization policy and engine power consumption. The engine map in the simulation was modified based on the empirical data in order to make it different from that of the vehicle in the market due to the data security purpose.

Fig. 5 shows the simulation results of the engine operating points for UDDS driving test cycle. Fig. 5 (a) and (b) are the results for DSHS and THS, respectively. The blue line in the figure shows the optimum operating line and the black line represents the maximum engine torque line. As shown in the figure, the operating points are located near the optimum operating line for both cases. This means that the simulation control optimization policy is well organized according to the given driving test cycle for both of them.

The difference between the two structures for the engine operating points is that DSHS uses an engine speed area
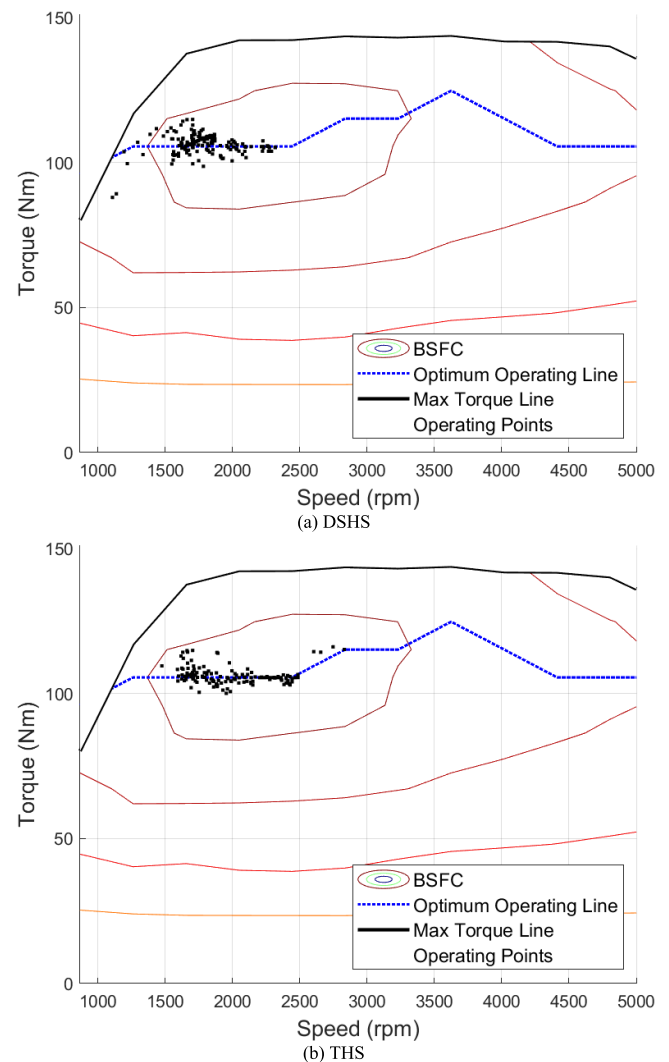

FIGURE 5. Simulation results of the engine operating points for UDDS driving test cycle, (a) DSHS and (b) THS.

between 1000 and 2300 rpm, while the engine speeds of THS are located between 1500 and 2900 rpm. This is due to that DSHS has more chances to choose lower engine speed with more driving modes in order to minimize the engine power consumption. As a result, DSHS consumes less fuel for UDDS driving test cycle than THS, because the engine power consumption gets lower with slow engine speed when the operating points are under the optimum operating line.

and the output-split power split hybrid mode is used for the relatively low power area near 40 km/h vehicle speed. On the other hand, THS utilizes the input-split power split hybrid mode for the high demand power area and the EV mode for the relatively low power area. We see that DSHS exploits multiple driving modes for the different velocity and wheel demand power conditions compared to THS.
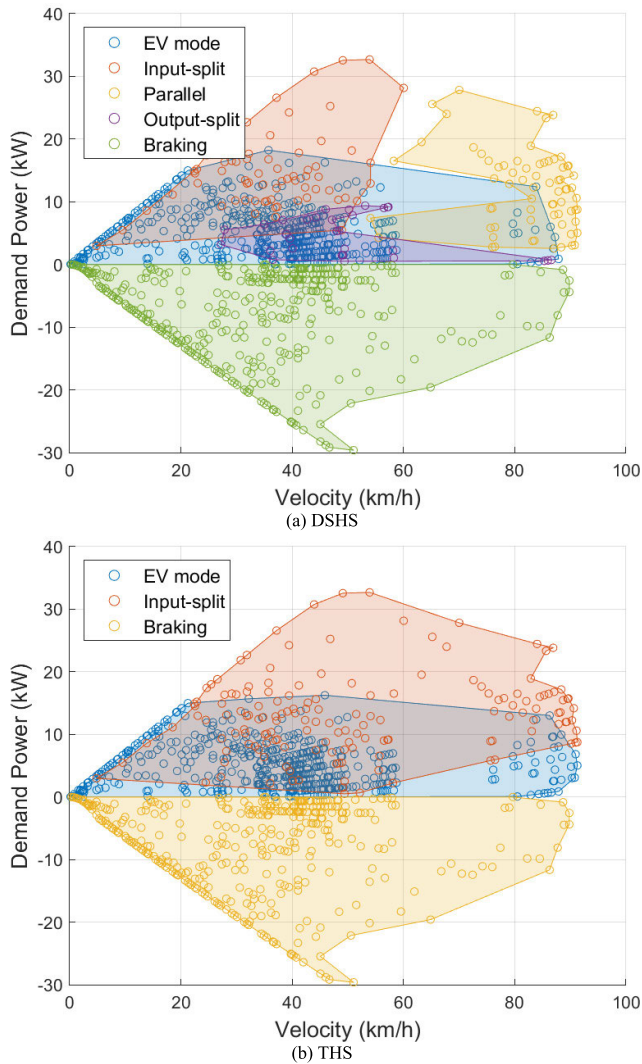
FIGURE 6. Simulation results of the operating modes according to the wheel demand power and velocity for UDDS, (a) DSHS and (b) THS.

FIGURE 7. Simulation results of the operating modes according to the wheel demand torque and velocity for UDDS, (a) DSHS and (b) THS.

The operating modes of the system were analyzed for the wheel demand power and torque with vehicle speeds. Fig. 6 shows the simulation results of the operating modes according to the wheel demand power and velocity for UDDS driving test cycle. Fig. 6 (a) and (b) show the results for DSHS and THS, respectively. For DSHS, all four driving modes are used for the given driving test cycle. The EV mode is used for the overall area, the input-split power split hybrid mode is used for the low speed and high demand power area, the parallel hybrid mode is used for the high speed area,
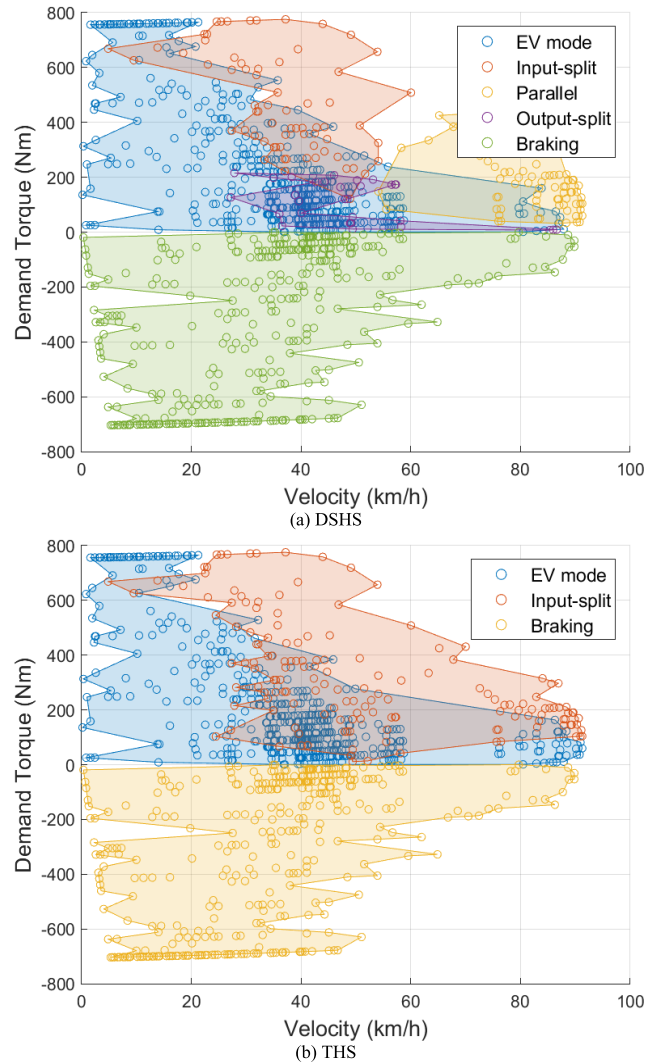
Fig. 7 shows the simulation results of the operating modes according to the wheel demand torque and velocity for UDDS driving teat cycle. Fig. 7 (a) and (b) are figures for DSHS and THS, respectively. As the operating modes on the velocity and wheel demand power map, DSHS additionally utilizes the parallel hybrid mode and output-split power split hybrid mode, while THS only has two driving modes for the given driving test cycle. The EV mode is exploited relatively slow velocity area, and the parallel hybrid mode is used for high velocity area. The input- and output- power split hybrid modes are mainly utilized for the velocity near 40 km/h.

Fig. 8 shows the simulation results of the SOC variations for UDDS driving test cycle. The initial SOC for both systems is set to 50 % and the final SOC is controlled by the optimal control strategy in order to have the same value as the initial SOC. The SOC variation range of DSHS is wider than that of THS. DSHS stores more energy into the battery compared to THS around between 200s and 800s, and utilizes it for the end of the driving test cycle. It shows that DSHS has more chance to store residual power from the engine by choosing a more efficient driving mode, and it utilizes the battery energy space more actively, which results in better fuel economy.
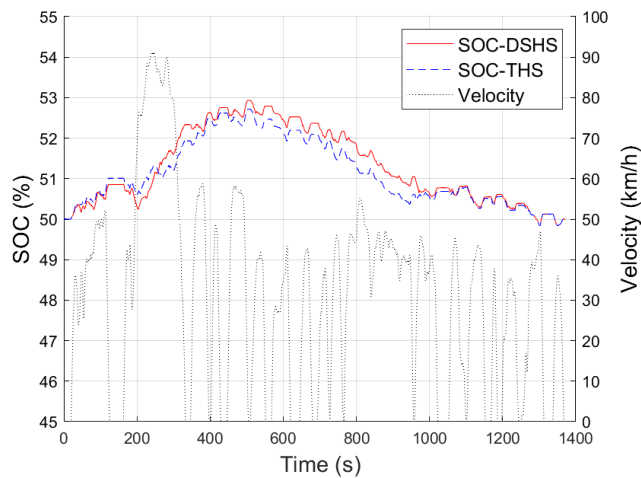
FIGURE 8. Simulation results of the SOC variations for UDDS.
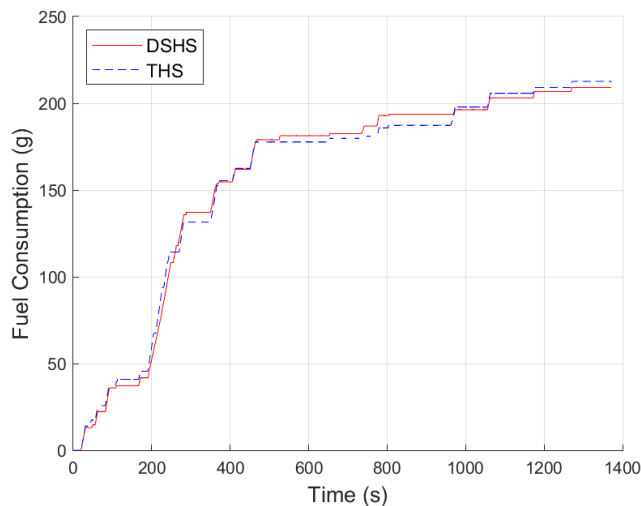
FIGURE 9. Simulation results of the accumulated fuel consumptions for UDDS.

Fig. 9 shows the simulation results of the accumulated fuel consumptions for UDDS driving test cycle. As expected, the engine for DSHS consumes more fuel energy between 200s and 800s. Even though the SOC variation range of DSHS is larger than that of THS, the final fuel consumption of DSHS is less than that of THS, since DSHS utilizes the residual space of the battery more actively using optimal control with

multiple driving modes. The overall fuel consumption of DSHS is 1.7 % less than THS with more opportunities for the driving modes.

The performance abilities of both given systems have been simulated and analyzed for HWFET driving test cycle. Fig. 10 (a) and (b) show the simulation results of the engine operating points for HWFET driving test cycle, for DSHS and THS, respectively. As the result of UDDS driving test cycle, the engine operating points of both systems are well positioned near the optimum operating line. The engine speed of DSHS is slightly lower than that of THS. The operating points of DSHS are mainly located between 1200 rpm and 2300 rpm, while those of THS are mainly placed between 1500 rpm and 2800 rpm of the engine speed. This is due to that DSHS has more opportunities to select the driving modes with low engine speed, which results in less engine power consumption for UDDS driving test cycle.

The schematics of operating modes for HWFET according to the wheel demand power and vehicle speed are shown
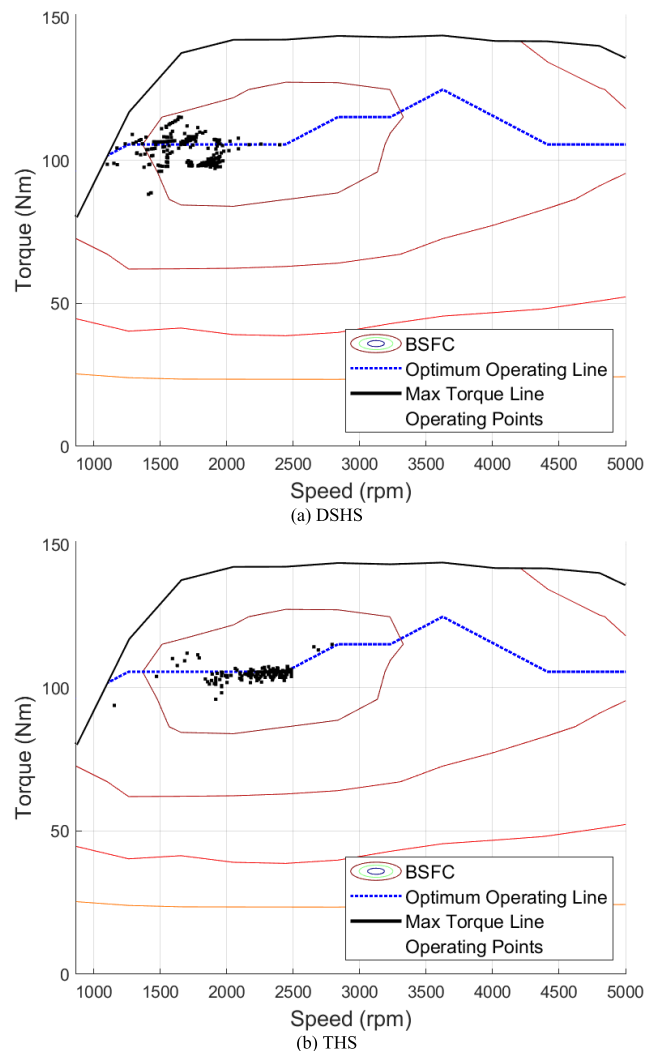

(a) DSHS

(b) THS

FIGURE 10. Simulation results of the engine operating points for HWFET, (a) DSHS and (b) THS.

in Fig. 11. Fig. 11 (a) and (b) show the results for DSHS and THS, respectively. For DSHS, mainly two driving modes are utilized for HWFET because the overall wheel demand power is lower than that for UDDS driving test cycle. The EV mode is used for the overall region, and the parallel hybrid mode is used for the high speed region, while the input- and output-split power split hybrid modes are rarely exploited, relatively. On the other hand, THS utilizes the input-split power split hybrid mode for the relatively high power area and the EV mode for the relatively low power with high speed area. We can see that the control strategies of both systems are totally different according to the possible operating modes for the given driving test cycle.
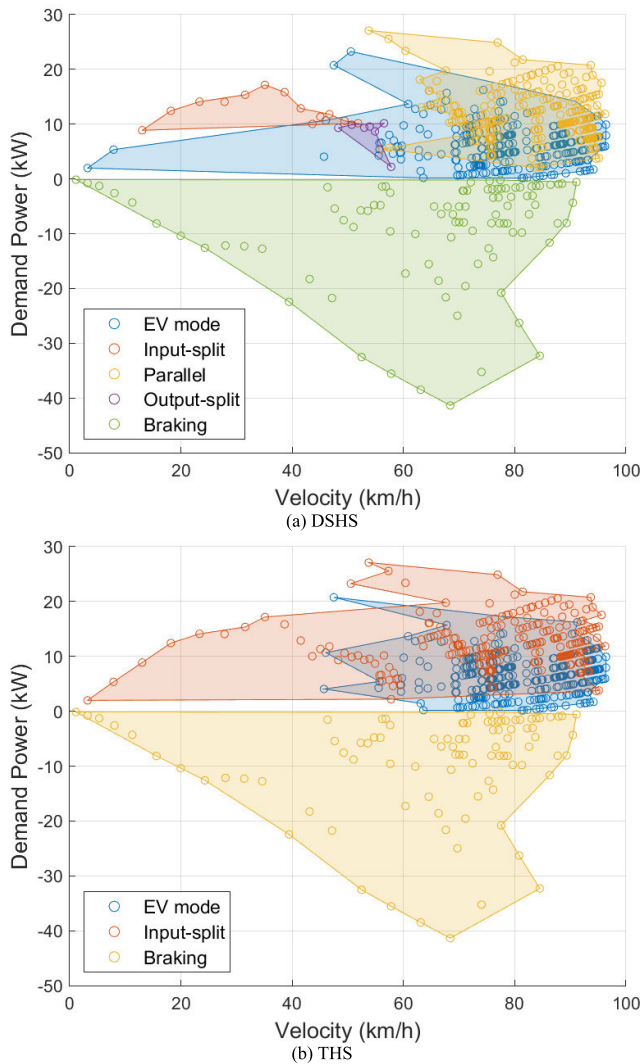
FIGURE 11. Simulation results of the operating modes according to the wheel demand power and velocity for HWFET, (a) DSHS and (b) THS.

Fig. 12 shows the simulation results of the operating modes according to the wheel demand torque and velocity for HWFET driving test cycle. Fig. 12 (a) and (b) are the results for DSHS and THS, respectively. Unlike the results for UDDS driving test cycle, the input-split and output power

split hybrid modes are hardly used for DSHS. The EV mode is mainly used for the low velocity and low torque area, while the parallel hybrid mode is mainly utilized for the high velocity with high demand torque area. According to the results, on the wheel demand power map, the main operating modes for DSHS are different from those for THS with a different control strategy. Both systems utilize different driving modes with the optimal control strategy in order to minimize fuel consumption and SOC balancing control.
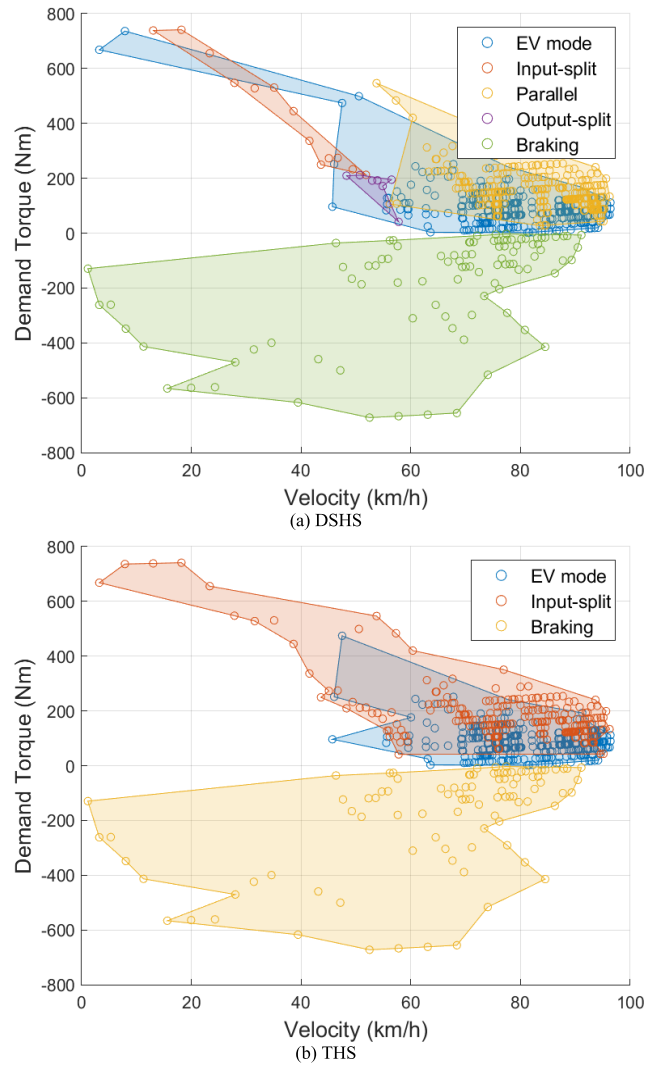

FIGURE 12. Simulation results of the operating modes according to the wheel demand torque and velocity for HWFET, (a) DSHS and (b) THS.

The simulation results of the SOC variations for HWFET driving test cycle are compared as in Fig. 13. The SOC starts from 50 % for both systems and the final SOC is set to the same as the initial SOC. Even though the variation trends for the first half of the driving test cycle are different, the trends are similar for the second half. According to Fig. 11 and 12, the DSHS uses mainly EV and parallel hybrid modes, while THS mainly uses EV and input-split hybrid modes. The difference of the main operating modes according to the

time makes the SOC balancing strategies different between both hybrid systems. As a result, different SOC balancing strategies result in different SOC variation trends.
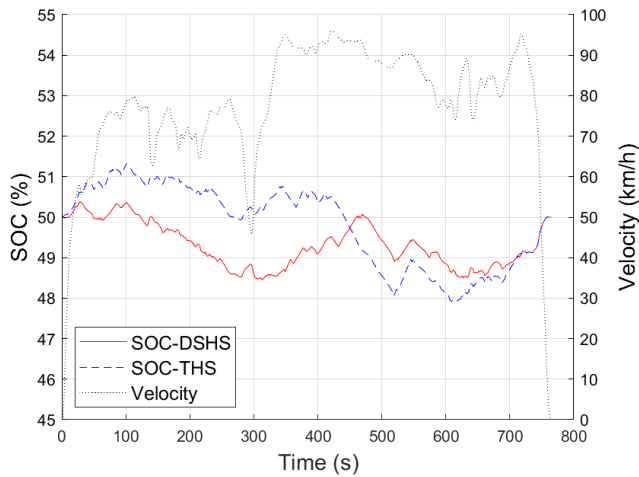

FIGURE 13. Simulation results of the SOC variations for HWFET.

Fig. 14 shows the simulation results of the accumulated fuel consumptions for HWFET driving test cycle. The trends of the accumulated fuel consumptions for both systems are similar since there are no big SOC variations for both systems. Even though the trends are similar, the overall fuel consumption of DSHS is 5% less than THS with more options of the driving modes for optimal system control.
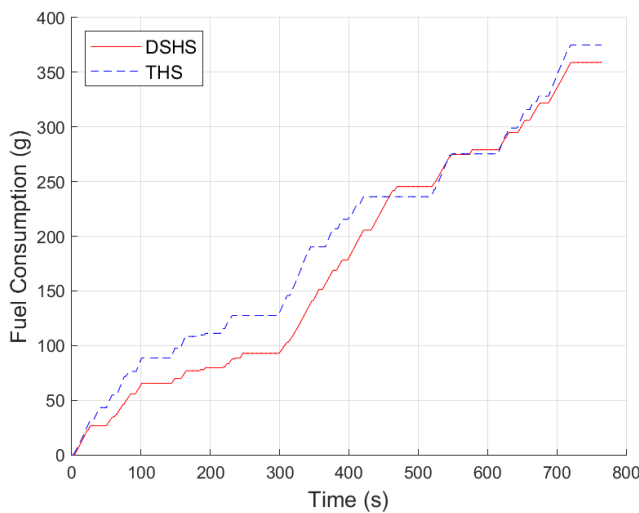

FIGURE 14. Simulation results of the accumulated fuel consumptions for HWFET.

According to the simulation results for UDDS and HWFET driving test cycles, DSHS shows better performance ability compared to THS in terms of the fuel economy for the given simulation conditions. The fuel energy consumptions for UDDS and HWFET driving test cycles are around 1.7 % and 4.5 % less than THS, respectively, even though the amount of the fuel consumption difference can be changed according

to the vehicle specifications. The operating modes of DSHS are more variable and it makes the engine and motor of the vehicle operating points located in a more efficient position.

B. COMPONENT SIZING

As well as the performance aspect, DSHS has a chance to reduce the size of electrical components by reducing the maximum power through the electrical path. During the design process of the system, the sizing of motors is determined with the maximum power and torque requirements for the test development process. If the maximum power and torque requirements are reduced, the motors can be designed smaller. For the design aspect of DSHS, the variation trend of speed and torque of motors were analyzed with assumptions that the vehicle velocity increases and the engine operates at a constant speed.

Fig. 15 shows the torque and speed variations of MG-1 when the vehicle velocity increases with a constant wheel demand torque. The torque for the output-split power split transmission is constant, while that for the input-split power split transmission increases along with increasing vehicle velocity. It results that the torque of the input-split power split transmission is lower than that of the output-split power split transmission when the motor speed is positive, and it becomes higher when the motor speed becomes negative. For DSHS, it can utilize the input-split power split hybrid mode for positive MG-1 speed and the output-split power split hybrid mode for negative MG-1 speed. As a result, the maximum required power of MG-1 for DSHS is smaller than the input-split power split transmission. It means that the maximum power and maximum torque of MG-1 for DSHS can be designed smaller compared to THS.

The component sizing of MG-2 can be analyzed as MG-1. Fig. 16 shows the torque and speed variations of MG-2 when the vehicle velocity increases with a constant wheel
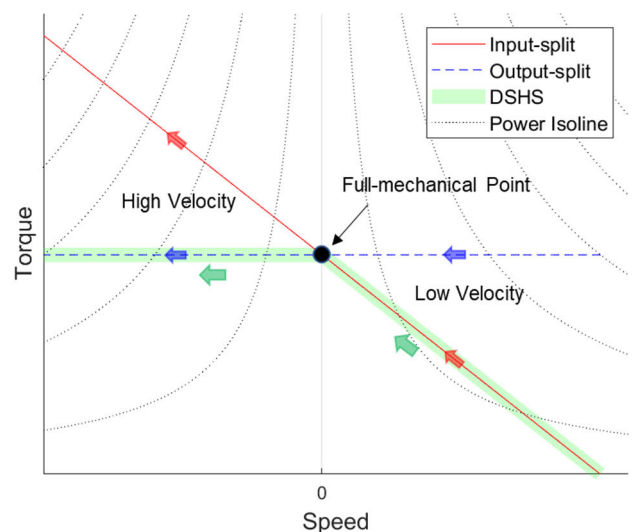

FIGURE 15. Torque and speed variations of MG-1 when the vehicle velocity increases with a constant wheel demand torque.
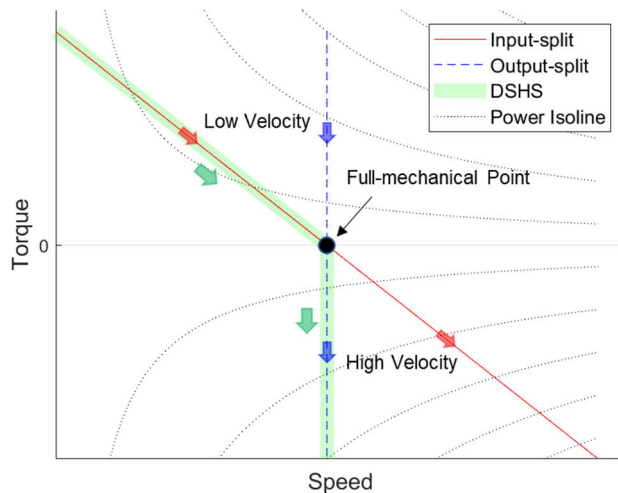
FIGURE 16. Torque and speed variations of MG-2 when the vehicle velocity increases with a constant wheel demand torque.

demand torque. The speed of MG-2 increases along with increasing vehicle velocity for the input-speed power split transmission. For the output-split power split transmission, the speed of MG-2 is constant since the engine speed is assumed as constant. As shown in the figure, when the vehicle velocity is slower than the full-mechanical point, the MG-2 for the output-slit power split transmission consumes more power, while the MG-2 for the input-split power split transmission requires higher power when the velocity becomes high. Since DSHS can select the input-split power split hybrid mode for the low velocity and the output-split power split hybrid mode for the high velocity, the maximum required power and torque for sizing the MG-2 can be reduced compared to other single mode power split systems.

In conclusion, DSHS shows the possibility of the reduction of component sizing for both MG-1 and MG-2 compared to other typical power split architectures by reducing the maximum torque and power requirements for the given example case. The sizing reduction of the motors affects not only the production cost reduction but also the vehicle packaging space minimization by reducing the physical volume of the motors, which can give an opportunity while producing vehicles by automotive manufacturers.

V. CONCLUSION

The invented novel multimode power split hybrid architecture based on input- and output-split power split hybrid modes has been studied by comparison with THS, which is a typical architecture of the power split hybrid systems. Both systems have been simulated by DP for UDDS and HWFET driving test cycles from EPA in order to compare the performance ability of the systems. In the result, the fuel consumption of DSHS shows around 1 to 5 % less than that of THS, even though the amount of difference depends on the vehicle specifications and driving test cycles. In addition, the component sizing aspect has been compared with an example case using constant wheel demand torque according to the

varying vehicle speeds. In the case study, DSHS shows more opportunities to select driving modes with lower demand power for motors compared to THS, because DSHS has more available modes for driving conditions. As a result, the size of the motors for DSHS can be smaller than that for THS. Since the component sizing affects not only the vehicle packaging space but also the cost of production, it can be said that the sizing aspect is one of the key factors for vehicle mass productions. In the simulation and case study, the DSHS shows better aspects in terms of fuel economy and component sizing. As future work, the given system can be analyzed further by other simulation methods and experimental studies.

REFERENCES

[1] S. A. Siffat, I. Ahmad, A. U. Rahman, and Y. Islam, "Robust integral backstepping control for unified model of hybrid electric vehicles," *IEEE Access*, vol. 8, pp. 49038–49052, 2020, doi: 10.1109/ACCESS.2020.2978258.

[2] S. Zhou, P. Walker, and N. Zhang, "Parametric design and regenerative braking control of a parallel hydraulic hybrid vehicle," *Mechanism Mach. Theory*, vol. 146, Apr. 2020, Art. no. 103714, doi: 10.1016/j.mechmachtheory.2019.103714.

[3] J. Kim, H. Kim, J. Bae, D. Kim, J. S. Eo, and K.-K. Kim, "Economic nonlinear predictive control for real-time optimal energy management of parallel hybrid electric vehicles," *IEEE Access*, vol. 8, pp. 177896–177920, 2020, doi: 10.1109/ACCESS.2020.3027024.

[4] Z. Song, X. Zhang, J. Li, H. Hofmann, M. Ouyang, and J. Du, "Component sizing optimization of plug-in hybrid electric vehicles with the hybrid energy storage system," *Energy*, vol. 144, pp. 393–403, Feb. 2018, doi: 10.1016/j.energy.2017.12.009.

[5] Y. Bai, J. Li, H. He, R. C. D. Santos, and Q. Yang, "Optimal design of a hybrid energy storage system in a plug-in hybrid electric vehicle for battery lifetime improvement," *IEEE Access*, vol. 8, pp. 142148–142158, 2020, doi: 10.1109/ACCESS.2020.3013596.

[6] C. Yang, S. You, W. Wang, L. Li, and C. Xiang, "A stochastic predictive energy management strategy for plug-in hybrid electric vehicles based on fast rolling optimization," *IEEE Trans. Ind. Electron.*, vol. 67, no. 11, pp. 9659–9670, Nov. 2020, doi: 10.1109/TIE.2019.2955398.

[7] H. Kim, T. Barhoumi, and D. Kum, "Comprehensive design methodology of compound-split hybrid electric vehicles: Introduction of the compound lever as a design tool," *IEEE Access*, vol. 7, pp. 84744–84756, 2019, doi: 10.1109/ACCESS.2019.2925146.

[8] H. Lee, C. Song, N. Kim, and S. W. Cha, "Comparative analysis of energy management strategies for HEV: Dynamic programming and reinforcement learning," *IEEE Access*, vol. 8, pp. 67112–67123, 2020, doi: 10.1109/ACCESS.2020.2986373.

[9] M. Cammalleri and A. Castellano, "Analysis of hybrid vehicle transmissions with any number of modes and planetary gearing: Kinematics, power flows, mechanical power losses," *Mechanism Mach. Theory*, vol. 162, Aug. 2021, Art. no. 104350, doi: 10.1016/j.mechmachtheory.2021.104350.

[10] N. Kim, N. Kim, and A. Rousseau, "Thermal model developments for electrified vehicles," *World Electr. Vehicle J.*, vol. 7, no. 1, pp. 114–120, Mar. 2015.

[11] B. Li, H. Kuo, X. Wang, Y. Chen, Y. Wang, D. Gerada, S. Worall, I. Stone, and Y. Yan, "Thermal management of electrified propulsion system for low-carbon vehicles," *Automot. Innov.*, vol. 3, no. 4, pp. 299–316, Dec. 2020, doi: 10.1007/s42154-020-00124-y.

[12] H. Kwon, M. Sprengel, and M. Ivantysynova, "Thermal modeling of a hydraulic hybrid vehicle transmission based on thermodynamic analysis," *Energy*, vol. 116, pp. 650–660, Dec. 2016, doi: 10.1016/j.energy.2016.10.001.

[13] H. Kwon and M. Ivantysynova, "Experimental and theoretical studies on energy characteristics of hydraulic hybrids for thermal management," *Energy*, vol. 223, May 2021, Art. no. 120033, doi: 10.1016/j.energy.2021.120033.

[14] X. Chen, J. Jiang, L. Zheng, H. Tang, and X. Chen, "Study and analysis of a multi-mode power split hybrid transmission," *World Electr. Vehicle J.*, vol. 11, no. 2, p. 46, Jun. 2020, doi: 10.3390/WEVJ11020046.

[15] F. Ju, W. Zhuang, L. Wang, and Z. Zhang, "Comparison of four-wheel-drive hybrid powertrain configurations," *Energy*, vol. 209, Oct. 2020, Art. no. 118286, doi: 10.1016/j.energy.2020.118286.

[16] H. Chen, L. Li, and F. Küçükay, "Study of series-parallel and power-split DHT for hybrid powertrains," *Automot. Innov.*, vol. 4, no. 1, pp. 23–33, Feb. 2021, doi: 10.1007/s42154-020-00126-w.

[17] H. Peng, D. Qin, J. Hu, and C. Fu, "Synthesis and analysis method for powertrain configuration of single motor hybrid electric vehicle," *Mechanism Mach. Theory*, vol. 146, Apr. 2020, Art. no. 103731, doi: 10.1016/j.mechmachtheory.2019.103731.

[18] T.-T. Ho and S.-J. Hwang, "Configuration synthesis of novel hybrid transmission systems using a combination of a ravigneaux gear train and a simple planetary gear train," *Energies*, vol. 13, no. 9, p. 2333, May 2020, doi: 10.3390/en13092333.

[19] F. Zhang, F. Yang, D. Xue, and Y. Cai, "Optimization of compound power split configurations in PHEV bus for fuel consumption and battery degradation decreasing," *Energy*, vol. 169, pp. 937–957, Feb. 2019, doi: 10.1016/j.energy.2018.12.059.

[20] N. Kim, S. Choi, J. Jeong, R. Vijayagopal, K. Stutenberg, and A. Rousseau, "Vehicle level control analysis for Voltec powertrain," *World Electr. Veh. J.*, vol. 9, no. 2, pp. 1–12, 2018, doi: 10.3390/wevj9020029.

[21] H. Kwon and M. Ivantysynova, "System characteristics analysis for energy management of power-split hydraulic hybrids," *Energies*, vol. 13, no. 7, p. 1837, Apr. 2020, doi: 10.3390/en13071837.

[22] F. Verbelen, W. Lhomme, E. Vinot, J. Stuyts, M. Vafaeipour, O. Hegazy, K. Stockman, and P. Sergeant, "Comparison of an optimized electrical variable transmission with the Toyota hybrid system," *Appl. Energy*, vol. 278, Nov. 2020, Art. no. 115616, doi: 10.1016/j.apenergy.2020.115616.

[23] X. Zhang, C.-T. Li, D. Kum, and H. Peng, "Prius$^+$ and Volt$^-$: Configuration analysis of power-split hybrid vehicles with a single planetary gear," *IEEE Trans. Veh. Technol.*, vol. 61, no. 8, pp. 3544–3552, Oct. 2012, doi: 10.1109/TVT.2012.2208210.

[24] M. I. Ramdan and K. A. Stelson, "Optimal design of a power-split hybrid hydraulic bus," *Proc. Inst. Mech. Eng., D, J. Automobile Eng.*, vol. 230, no. 12, pp. 1699–1718, Oct. 2016, doi: 10.1177/0954407015621817.

[25] X. Hu, H. Zhang, D. Ma, R. Wang, and P. Tu, "Small leak location for intelligent pipeline system via action-dependent heuristic dynamic programming," *IEEE Trans. Ind. Electron.*, early access, Nov. 16, 2021, doi: 10.1109/TIE.2021.3127016.

[26] G. Mohan, F. Assadian, and S. Longo, "Comparative analysis of forward-facing models vs backward-facing models in powertrain component sizing," in *Proc. Hybrid Electr. Vehicles Conf. (HEVC)*, 2013, pp. 1–6, doi: 10.1049/cp.2013.1920.

[27] EPA. *Data on Cars used for Testing Fuel Economy*. [Online]. Available: https://www.epa.gov/compliance-and-fuel-economy-data/data-cars-used-testing-fuel-economy

[28] P. G. Anselma, A. Biswas, G. Belingardi, and A. Emadi, "Rapid assessment of the fuel economy capability of parallel and series-parallel hybrid electric vehicles," *Appl. Energy*, vol. 275, Oct. 2020, Art. no. 115319, doi: 10.1016/j.apenergy.2020.115319.

[29] R. Bellman, *Dynamic Programming*. New York, NY, USA: Dover, 1957.

[30] Y. Yang, X. Hu, H. Pei, and Z. Peng, "Comparison of power-split and parallel hybrid powertrain architectures with a single electric machine: Dynamic programming approach," *Appl. Energy*, vol. 168, pp. 683–690, Apr. 2016, doi: 10.1016/j.apenergy.2016.02.023.

[31] D. E. Kirk, *Optimal Control Theory: An Introduction*. New York, NY, USA: Dover, 1970.

[32] P. Polverino, I. Arsie, and C. Pianese, "Optimal energy management for hybrid electric vehicles based on dynamic programming and receding horizon," *Energies*, vol. 14, no. 12, p. 3502, Jun. 2021, doi: 10.3390/en14123502.

HYUKJOON KWON received the B.S. and M.S. degrees in mechanical and aerospace engineering from Seoul National University, Seoul, South Korea, and the Ph.D. degree in mechanical engineering from Purdue University, West Lafayette, IN, USA. Currently, he is a Senior Research Engineer at Hyundai Motor Company Research and Development Center, South Korea. His research interests include eco-friendly systems and advanced electrified drive systems for future mobility, such as hybrid vehicles, electric vehicles, and purpose-built vehicles.

YEONGIL CHOI received the B.S. and M.S. degrees in mechanical and aerospace engineering from Seoul National University, Seoul, South Korea. Currently, he is a Senior Research Engineer at Hyundai Motor Company Research and Development Center, South Korea.

WOULSUN CHOI received the B.S. and M.S. degrees in mechanical engineering from Sungkyunkwan University, South Korea. Currently, she is a Senior Research Engineer at Hyundai Motor Company Research and Development Center, South Korea.

SEUNGWOOK LEE received the B.S. degree in mechanical engineering from Yonsei University, South Korea. Currently, he is a Research Engineer at Hyundai Motor Company Research and Development Center, South Korea.

⚫ ⚫ ⚫